

CERN-EP-2022-041  
11 March 2022

## Underlying-event properties in pp and p–Pb collisions at $\sqrt{s_{\text{NN}}} = 5.02$ TeV

ALICE Collaboration

### Abstract

We report about the properties of the underlying event measured with ALICE at the LHC in pp and p–Pb collisions at  $\sqrt{s_{\text{NN}}} = 5.02$  TeV. The event activity, quantified by charged-particle number and summed- $p_{\text{T}}$  densities, is measured as a function of the leading-particle transverse momentum ( $p_{\text{T}}^{\text{trig}}$ ). These quantities are studied in three azimuthal-angle regions relative to the leading particle in the event: toward, away, and transverse. Results are presented for three different  $p_{\text{T}}$  thresholds (0.15, 0.5 and 1 GeV/c) at mid-pseudorapidity ( $|\eta| < 0.8$ ). The event activity in the transverse region, which is the most sensitive to the underlying event, exhibits similar behaviour in both pp and p–Pb collisions, namely, a steep increase with  $p_{\text{T}}^{\text{trig}}$  for low  $p_{\text{T}}^{\text{trig}}$ , followed by a saturation at  $p_{\text{T}}^{\text{trig}} \approx 5$  GeV/c. The results from pp collisions are compared with existing measurements at other centre-of-mass energies. The quantities in the toward and away regions are also analyzed after the subtraction of the contribution measured in the transverse region. The remaining jet-like particle densities are consistent in pp and p–Pb collisions for  $p_{\text{T}}^{\text{trig}} > 10$  GeV/c, whereas for lower  $p_{\text{T}}^{\text{trig}}$  values the event activity is slightly higher in p–Pb than in pp collisions. The measurements are compared with predictions from the PYTHIA 8 and EPOS LHC Monte Carlo event generators.

arXiv:2204.10389v1 [nucl-ex] 21 Apr 2022

## 1 Introduction

In non-diffractive proton–proton (pp) collisions at high energies, the underlying event (UE) consists of the set of particles that arise from the proton break-up (beam remnants), and from other semi-hard scatterings, in a scenario of multiparton interactions (MPI) [1]. The UE activity accompanies high transverse momentum ( $p_{\text{T}}$ ) particles produced by the main partonic scattering (jets). Experimental studies aimed at probing the UE component are commonly performed in azimuthal-angle regions where the contribution from the hard scattering is expected to be minimal. The present study follows the strategy originally introduced by the CDF collaboration [2]. Firstly, the leading particle (or trigger particle) in the event is found, i.e., the charged particle with the highest transverse momentum in the collision ( $p_{\text{T}}^{\text{trig}}$ ). Secondly, the associated particles for three different thresholds of the transverse momentum,  $p_{\text{T}} > 0.15, 0.5,$  and  $1$  GeV/ $c$ , are grouped in three classes depending on their relative azimuthal angle with respect to the leading particle,  $|\Delta\phi| = |\phi^{\text{assoc}} - \phi^{\text{trig}}|$ :

- toward:  $|\Delta\phi| < 60^\circ$ ,
- transverse:  $60^\circ < |\Delta\phi| < 120^\circ$ , and
- away:  $|\Delta\phi| > 120^\circ$ .

The three topological regions corresponding to the azimuthal-angle intervals defined above are illustrated in Fig. 1. The toward region contains the primary jet of the collision, while the away region contains the recoiled jet [3]. In contrast, the transverse region is mostly dominated by the UE dynamics, but it also includes contributions from initial- and final-state radiation (ISR and FSR) [4]. This strategy [2] has been used by several experiments at RHIC [5], the Tevatron [2, 6–8], and the LHC [9–14]. The studies include measurements in events with Drell–Yan [15] and Z-boson [16–18] production.

Experimental results have shown that the event activity, quantified by charged-particle number or summed- $p_{\text{T}}$  densities, in the transverse region rises steeply with increasing  $p_{\text{T}}^{\text{trig}}$  at low  $p_{\text{T}}^{\text{trig}}$  ( $< 5$  GeV/ $c$ ), and then it roughly saturates (plateau) for larger  $p_{\text{T}}^{\text{trig}}$  [14]. This saturation is expected in models that include the concept of impact parameter such that the requirement of the presence of a high- $p_{\text{T}}$  particle in a pp collision biases the selection of collisions towards those with a small impact parameter [19]. Based on UE observables measured at LHC centre-of-mass energies,  $\sqrt{s} = 0.9, 7,$  and  $13$  TeV, the event activity in the plateau region has been found to increase faster with increasing  $\sqrt{s}$  than in minimum-bias pp collisions [11, 14]. An analogous study for p–Pb collisions has never been performed, although an attempt to determine the correlation between the impact parameter of the collision and the charged-particle multiplicity has been reported [20].

The measurements performed at RHIC and LHC in pp, p–A, and d–A collisions have shown for high-particle multiplicities similar phenomena as were originally observed only in A–A collisions and have been attributed there to collective effects [21]. Thus, investigating pp and p–Pb collisions has become ever more pertinent in order to understand the origin of these effects [21–26]. In QCD (quantum chromodynamics)-inspired Monte Carlo (MC) generators like PYTHIA 8 [27], outgoing partons originating from MPI are allowed to interact with those from the main partonic scattering. This mechanism, known as colour reconnection, produces effects resembling collective behaviour in pp collisions [28]. Given the dynamics encoded in the transverse region, the colour reconnection effects are expected to be more relevant in such a topological region [29]. Therefore, beyond the importance of UE measurements for MC tuning [30, 31], the study of the event activity in the transverse region is important to contribute to the understanding of the new effects observed in high-multiplicity pp and p–Pb collisions [32].

In this paper, measurements of the event activity as a function of  $p_{\text{T}}^{\text{trig}}$  in pp and p–Pb collisions at the same centre-of-mass energy per nucleon pair ( $\sqrt{s_{\text{NN}}} = 5.02$  TeV) are reported. The event activity

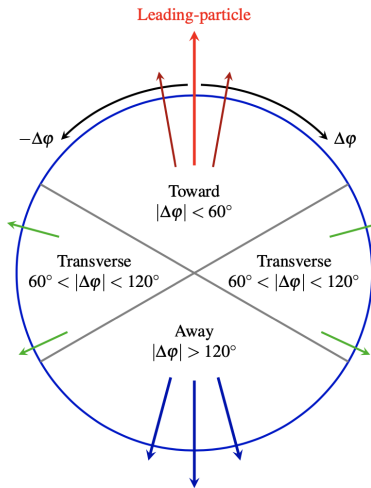


**Figure 1:** Illustration of the toward, transverse, and away regions in the azimuthal plane with respect to the leading particle direction. The figure has been taken from Ref. [14].

for each topological region in p–Pb collisions is compared with that in pp collisions at the same  $p_T^{\text{trig}}$ . In order to search for a possible system size dependence of the jet-like particle densities, the jet-like signal (in the toward and away regions) is further isolated by subtracting the UE contribution estimated from the transverse region. The results from pp collisions are compared to predictions from the EPOS tune LHC [33] and PYTHIA 8.244 (Monash 2013 tune [30]) Monte Carlo event generators, hereinafter referred to as EPOS LHC and PYTHIA 8/Monash, respectively. For p–Pb collisions, data are compared to EPOS LHC and PYTHIA 8/Angantyr [34].

For pp collisions, the modelling of UE in PYTHIA 8/Monash considers an impact-parameter dependent MPI activity. The partonic configuration is hadronised using string fragmentation as described by the Lund string model [35], followed by the decays of unstable particles. In collisions with several MPI, individual long strings connected to the remnants are replaced by shorter additional strings connecting partons from different semi-hard scatterings (colour reconnection). The Monash 2013 tune used minimum-bias, Drell-Yan, and UE data from the LHC to constrain the initial-state radiation and multiparton interactions, combined with data from the SPS and the Tevatron to constrain the scaling with the collision energy. The simulation of p–Pb collisions was performed with the recent model named Angantyr [34], which is based on an extrapolation of pp dynamics with a minimum number of free parameters. The model does not assume the formation of a hot thermalised medium, instead, the generalisation to collisions involving nuclei is inspired by the Fritiof model [36] and the notion of “wounded” or “participating” nucleons. The number of wounded nucleons is calculated from the Glauber model in impact parameter space. With these assumptions, the model is able to give a good description of general final-state properties such as multiplicity and transverse momentum distributions of particles produced in interactions involving heavy nuclei.

In EPOS LHC, the description of multiple partonic scatterings is based on a combination of Gribov-Regge theory and pQCD [37]. An elementary scattering corresponds to a parton ladder, containing a hard scattering which is calculated based on pQCD, including initial- and final-state radiation. Parton ladders that are formed in parallel to each other share the total collision energy leading to consistent treatment of energy conservation in hadronic collisions. String hadronisation in EPOS is based on the local density of the string segments per unit volume with respect to a critical-density parameter. Event-by-event, string segments in low-density regions hadronise normally and independently, creating the so-called corona, while string segments in high-density regions are used to create a core with collective expansion resulting in radial and longitudinal flow effects. The EPOS LHC tune considered here is based

on a dedicated parameter set used to describe data from different centre-of-mass energies and collision systems at the LHC.

The paper is organised as follows. The ALICE detectors used in the analysis are described in Section 2. Section 3 is dedicated to illustrate the analysis technique, the data correction procedures, and the evaluation of the systematic uncertainties. The results are presented and discussed in Section 4, and the conclusions are summarised in Section 5.

## 2 Experimental setup

The main ALICE detectors used in the present work are the Inner Tracking System (ITS), the Time Projection Chamber (TPC), and the V0 detector. The ITS and TPC detectors are both used for primary vertex and track reconstruction. The V0 detector is used for triggering and for beam background rejection. More details concerning the ALICE detector system and its performance can be found in Refs. [38, 39].

The ITS and TPC detectors are the main tracking devices covering the pseudorapidity region  $|\eta| < 0.8$  for full-length tracks. They are located inside a solenoidal magnet providing a 0.5 T magnetic field, allowing the tracking of particles with  $p_{\text{T}} \gtrsim 0.15$  GeV/ $c$ . The ITS is composed of six cylindrical layers of high-resolution silicon tracking detectors. The innermost layers consist of two arrays of hybrid Silicon Pixel Detectors (SPD) located at an average radial distance of 3.9 cm and 7.6 cm from the beam axis and covering  $|\eta| < 2$  and  $|\eta| < 1.4$ , respectively. The TPC has an active radial range from about 85 to 250 cm, and an overall length along the beam direction of 500 cm. The TPC readout chambers have 159 tangential pad rows and thus a charged particle can, ideally, produce 159 clusters within the TPC volume. The readout chambers are mounted into 18 trapezoidal sectors at each end plate [39]. The V0 detector consists of two sub-detectors placed on each side of the interaction point covering the full azimuthal acceptance and the pseudorapidity intervals of  $2.8 < \eta < 5.1$  (V0A) and  $-3.7 < \eta < -1.7$  (V0C).

This analysis is based on the data recorded by the ALICE apparatus during the pp run at  $\sqrt{s} = 5.02$  TeV in 2015, and the p–Pb run at  $\sqrt{s_{\text{NN}}} = 5.02$  TeV in 2016. The data were collected using a minimum-bias trigger, which required a signal in both V0A and V0C detectors. Only events with a reconstructed vertex within  $\pm 10$  cm from the nominal interaction point along the beam direction are used. Events with collision pile-up are identified and rejected based on the presence of multiple interaction vertices reconstructed using the SPD information. The offline event selection is optimised to reject beam-induced background by exploiting the timing signals in the two V0 sub-detectors. The event selection also requires at least one track with a minimum transverse momentum ( $p_{\text{T}} = 0.15, 0.5, \text{ and } 1.0$  GeV/ $c$ ) in the acceptance range  $|\eta| < 0.8$ . The results presented in this article were obtained from the analysis of about 180 and 332 million minimum-bias pp and p–Pb collisions, respectively.

## 3 Analysis details

### 3.1 Track reconstruction and selection

The event properties are studied from the number and the momenta of the primary charged particles in the pseudorapidity interval  $|\eta| < 0.8$ . Primary particles are defined as particles with a mean proper lifetime larger than 1 cm/ $c$ , which are either produced directly in the interaction or from decays of particles with a mean proper lifetime smaller than 1 cm/ $c$  [40]. Charged particles are reconstructed with the ITS and TPC detectors, providing a measurement of the track transverse momentum  $p_{\text{T}}$  and azimuthal angle  $\phi$ , which are used in the analysis. Tracks are required to have at least two hits in the ITS detector, of which at least one in either of the two innermost layers. The ratio of crossed TPC pad rows to the number of findable TPC clusters is required to be larger than 0.8, and the fraction of TPC clusters shared with another track should be less than 0.4. In addition, tracks are required to have a number of crossed TPC pad rows larger than  $0.85 \times L$ , where  $L$  (in cm) is the geometrical track length calculated in the TPC readout plane,

excluding the information from the pads at the sector boundaries ( $\approx 3$  cm from the sector edges). The number of TPC clusters associated to the track is required to be larger than  $0.7 \times L$ . The fit quality for the ITS and TPC track points must satisfy  $\chi_{\text{ITS}}^2/N_{\text{hits}} < 36$  and  $\chi_{\text{TPC}}^2/N_{\text{clusters}} < 4$ , respectively, where  $N_{\text{hits}}$  and  $N_{\text{clusters}}$  are the number of hits in the ITS and the number of clusters in the TPC, respectively. To select primary particles, tracks having a large distance of closest approach (DCA) to the reconstructed vertex in the longitudinal ( $d_z > 2$  cm) and radial ( $d_{xy} > 0.018 \text{ cm} + 0.035 \text{ cm} \times (\text{GeV}/c) \times p_{\text{T}}^{-1}$ ) directions are rejected. To further reduce the contamination from secondary particles, only tracks with  $\chi_{\text{TPC-ITS}}^2 < 36$  are included in the analysis, where  $\chi_{\text{TPC-ITS}}^2$  is calculated by comparing the track parameters from the combined ITS and TPC track reconstruction to those derived only from the TPC and constrained by the interaction point [41].

### 3.2 Underlying-event observables

The transverse momentum spectra ( $p_{\text{T}}$ ) as a function of  $p_{\text{T}}^{\text{trig}}$  are corrected for all  $p_{\text{T}}^{\text{trig}}$  intervals and are extracted for each topological region. Then, both the primary charged-particle number and the summed transverse-momentum densities are calculated from the  $p_{\text{T}}$  spectra. The event activity in each topological region is measured as a function of  $p_{\text{T}}^{\text{trig}}$ . It is quantified with the primary charged-particle number density:

$$\left\langle \frac{d^2 N_{\text{ch}}}{d\eta d\phi} \right\rangle (p_{\text{T}}^{\text{trig}}) = \frac{1}{\Delta\eta\Delta\phi} \frac{1}{N_{\text{ev}}(p_{\text{T}}^{\text{trig}})} N_{\text{ch}}(p_{\text{T}}^{\text{trig}}), \quad (1)$$

and the summed transverse-momentum density:

$$\left\langle \frac{d^2 \sum p_{\text{T}}}{d\eta d\phi} \right\rangle (p_{\text{T}}^{\text{trig}}) = \frac{1}{\Delta\eta\Delta\phi} \frac{1}{N_{\text{ev}}(p_{\text{T}}^{\text{trig}})} \sum p_{\text{T}}(p_{\text{T}}^{\text{trig}}), \quad (2)$$

where  $N_{\text{ev}}(p_{\text{T}}^{\text{trig}})$  is the total number of events with the leading particle in a given  $p_{\text{T}}^{\text{trig}}$  interval;  $N_{\text{ch}}(p_{\text{T}}^{\text{trig}})$  and  $\sum p_{\text{T}}(p_{\text{T}}^{\text{trig}})$  stand for multiplicity and sum of the  $p_{\text{T}}$  of all reconstructed tracks within a given topological region, respectively. Finally,  $\Delta\eta$  is the pseudorapidity interval used in the analysis.

This paper also reports the charged-particle number and the summed- $p_{\text{T}}$  densities in the toward and away regions after the subtraction of the event activity in the transverse region. All these quantities are measured as a function of  $p_{\text{T}}^{\text{trig}}$ .

The charged-particle number density in the jet-like signal is derived from the difference between the number density in the toward (or away) region and that in the transverse region:

$$\left\langle \frac{d^2 N_{\text{ch}}}{d\eta d\phi} \right\rangle^{\text{jet toward(away)}} (p_{\text{T}}^{\text{trig}}) = \left[ \left\langle \frac{d^2 N_{\text{ch}}}{d\eta d\phi} \right\rangle^{\text{toward(away)}} - \left\langle \frac{d^2 N_{\text{ch}}}{d\eta d\phi} \right\rangle^{\text{transverse}} \right] (p_{\text{T}}^{\text{trig}}). \quad (3)$$

In the same way, the summed- $p_{\text{T}}$  density in the jet-like signal is obtained as follows:

$$\left\langle \frac{d^2 \sum p_{\text{T}}}{d\eta d\phi} \right\rangle^{\text{jet toward(away)}} (p_{\text{T}}^{\text{trig}}) = \left[ \left\langle \frac{d^2 \sum p_{\text{T}}}{d\eta d\phi} \right\rangle^{\text{toward(away)}} - \left\langle \frac{d^2 \sum p_{\text{T}}}{d\eta d\phi} \right\rangle^{\text{transverse}} \right] (p_{\text{T}}^{\text{trig}}). \quad (4)$$

The ratio between these two quantities gives the average transverse momentum in the jet-like signal:

$$\langle p_{\text{T}} \rangle^{\text{jet toward(away)}} = \left\langle \frac{d^2 \sum p_{\text{T}}}{d\eta d\phi} \right\rangle^{\text{jet toward(away)}} \left/ \left\langle \frac{d^2 N_{\text{ch}}}{d\eta d\phi} \right\rangle^{\text{jet toward(away)}} \right. . \quad (5)$$

### 3.3 Corrections

The correction of  $p_{\text{T}}$  spectra of charged particles follows the standard procedure of the ALICE collaboration [42, 43]. The raw yields are corrected for efficiency and contamination from secondary particles. The efficiency correction is calculated from Monte Carlo simulations including the propagation of particles through the detector using GEANT 3 [44]. For pp and p–Pb collisions the PYTHIA 8 and EPOS LHC Monte Carlo event generators are used for this purpose, respectively. As the relative abundances of different charged particle species are different in the data and in the simulations, the efficiency obtained from the simulations is re-weighted considering the primary charged particle composition measured by ALICE [45], as described in Ref. [43]. The residual contamination from secondary particles in the sample of selected tracks is estimated via a fit to the measured  $d_{\text{xy}}$  distributions by a combination of the  $d_{\text{xy}}$  distributions (templates) of primary and secondary particles obtained from the simulations [43].

Due to the finite acceptance and the efficiency of the detection apparatus, the leading particle may not be detected, and a track with lower  $p_{\text{T}}$  could be considered as the trigger particle. If the misidentified leading particle has a different  $p_{\text{T}}$  but roughly the same direction as the true leading particle, this leads to a small effect on the UE observables [11]. On the other hand, if the misidentified leading particle has a significantly different direction than the true one, this will cause a rotation of the event topology and a bias on the UE observables. Therefore, the particle densities are corrected for these effects using a data-driven procedure described in detail in Ref. [11]. A minor correction due to the finite vertex reconstruction efficiency is also applied to the UE observables.

**Table 1:** Main sources and values of the relative systematic uncertainties of the charged-particle number and summed- $p_{\text{T}}$  densities in pp and p–Pb collisions at  $\sqrt{s_{\text{NN}}} = 5.02$  TeV. The average values of the uncertainties for the  $p_{\text{T}}^{\text{trig}}$  intervals 0.5–2 GeV/c and 5–40 GeV/c are displayed in the left and right columns, respectively. These uncertainties correspond to the transverse momentum threshold  $p_{\text{T}} > 0.5$  GeV/c. When more than one number is quoted, the values refer to the uncertainty in toward, transverse, and away regions, respectively; they are independent of the azimuthal region in all other cases.

<b>pp collisions</b>	Number density		Summed- $p_{\text{T}}$ density	
	$p_{\text{T}}^{\text{trig}} < 2$ GeV/c	$p_{\text{T}}^{\text{trig}} > 5$ GeV/c	$p_{\text{T}}^{\text{trig}} < 2$ GeV/c	$p_{\text{T}}^{\text{trig}} > 5$ GeV/c
Sec. contamination	0.4%	negligible	0.4%	negligible
Correction method	3.7%, 3.5%, 3.3%	1.7%, 0.1%, 0.6%	1.8%, 1.5%, 1.6%	2.0%, 0.2%, 0.3%
Track cuts	2.1%	2.8%	2.1%	2.9%
ITS-TPC track matching	0.9%	0.8%	0.9%	0.8%
Misidentification bias	2.3%	negligible	2.8%	0.2%
Event selection	negligible	negligible	negligible	negligible
Total uncertainty	4.9%, 4.8%, 4.6%	3.4%, 2.9%, 3.0%	4.1%, 3.9%, 4.0%	3.6%, 3.0%, 3.0%
<b>p–Pb collisions</b>	Number density		Summed- $p_{\text{T}}$ density	
	$p_{\text{T}}^{\text{trig}} < 2$ GeV/c	$p_{\text{T}}^{\text{trig}} > 5$ GeV/c	$p_{\text{T}}^{\text{trig}} < 2$ GeV/c	$p_{\text{T}}^{\text{trig}} > 5$ GeV/c
Sec. contamination	0.5%	negligible	0.4%	negligible
Correction method	2.1%, 2.0%, 2.0%	0.8%, 0.6%, 0.7%	0.8%, 0.6%, 0.7%	0.9%, negl., 0.1%
Track cuts	1.5%	3.1%	1.4%	3.2%
ITS-TPC track matching	1.8%	2.0%	1.9%	2.0%
Misidentification bias	3.9%	0.1%	1.8%	0.2%
Event selection	negligible	negligible	negligible	negligible
Total uncertainty	5.0%, 5.0%, 5.0%	3.8%, 3.7%, 3.8%	3.1%, 3.1%, 3.1%	3.9%, 3.8%, 3.8%

### 3.4 Systematic uncertainties

The relative systematic uncertainties on the quantities presented in Eqs. 1, 2, 3, 4, and 5 are summarised in Table 1 for pp and p–Pb collisions. The details about the different conditions varied in the analysis to estimate the systematic uncertainties are described below.

- Secondary contamination: the fits to the  $d_{xy}$  distributions with the templates from the simulations were repeated using different fit intervals, namely  $-1 < d_{xy} < 1$  cm and  $-2 < d_{xy} < 2$  cm, instead of the default interval  $-3 < d_{xy} < 3$  cm. The maximum deviation with respect to the result obtained with the default fit range was assigned as systematic uncertainty.
- Correction method: a possible bias introduced by imperfections in the correction procedure was estimated by performing the analysis on a Monte Carlo sample of pp collisions simulated with a given event generator. The generated particles were propagated through the detector and the reconstructed quantities were corrected with the same procedure applied to the real data utilising the correction factors extracted from simulations performed with the same event generator. With this approach, one expects to reproduce the generated yields within statistical uncertainty. This consideration holds only if each correction is evaluated with respect to all the variables to which the given correction is sensitive. Any statistically significant difference between input and corrected distributions is added in quadrature to the total systematic uncertainty. This uncertainty is the only one which is different for each topological region.
- Track selection: the systematic uncertainty related to the track selection criteria was determined by varying the track quality cuts [42, 43]. In particular, the upper limits of the track fit quality parameters in the ITS ( $\chi_{\text{ITS}}^2/N_{\text{hits}}$ ) and the TPC ( $\chi_{\text{TPC}}^2/N_{\text{clusters}}$ ) were varied in the ranges of 25–49 and 3–5, respectively. The minimum ratio of crossed TPC pad rows to the number of findable TPC clusters was varied within (0.7–0.9). The maximum fraction of shared TPC clusters was varied between 0.2 and 1, and the maximum  $d_z$  was varied within 1–5 cm. The impact on the results due to the hit requirement in the SPD was also evaluated by removing that requirement from the track selection. The maximum deviation of the results obtained varying the selections (only a single track cut at a time) with respect to the result obtained using the default track selection criteria was assigned as systematic uncertainty on each individual track-quality variable. The total uncertainty is then calculated as the sum in quadrature of each contribution.
- ITS-TPC track matching efficiency: a systematic uncertainty on the track reconstruction efficiency originates from possible differences in the probability to match the TPC tracks to the ITS hits in data and in simulations. It was estimated by comparing the matching efficiency in data and simulations and propagating their difference to the underlying-event observables used in the analysis.
- Leading-particle misidentification bias: the uncertainty on the leading-track misidentification correction is estimated from the discrepancy between the data-driven correction used in the analysis and the correction obtained from simulated data where the true leading particle is known.
- Event-selection bias: the systematic uncertainty due to event selection is obtained by varying from 5 to 15 cm the cut on the absolute value of the  $z$  component of the vertex position. The maximum deviation of the results obtained varying the vertex position with respect to the result obtained using the default cut (10 cm) is assigned as systematic uncertainty. This contribution is found to be negligible.

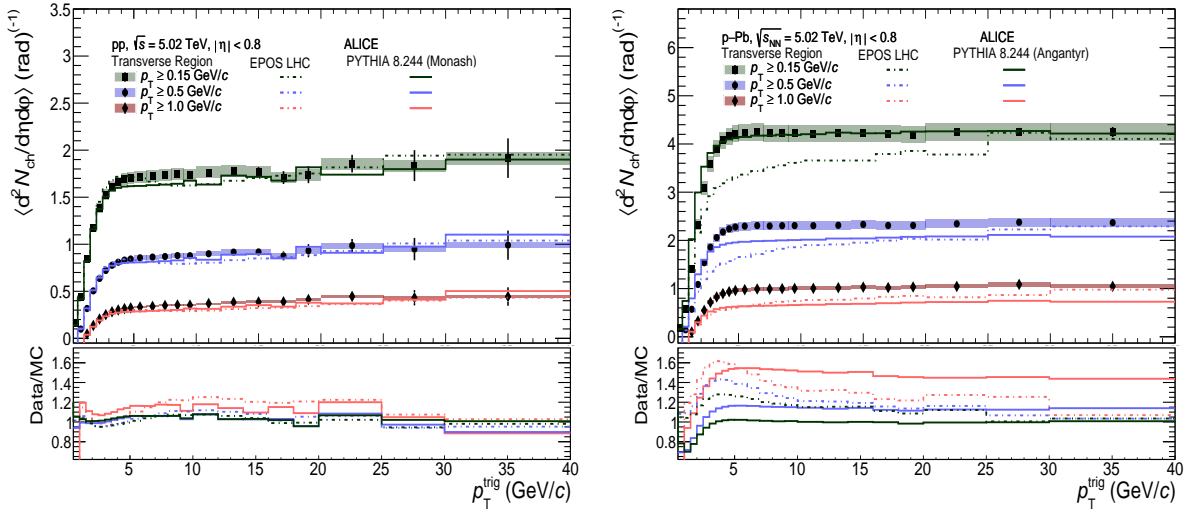


**Figure 2:** Charged-particle number density as a function of  $p_{\text{T}}^{\text{trig}}$  measured in the transverse region for pp (left) and p–Pb collisions (right) at  $\sqrt{s_{\text{NN}}} = 5.02$  TeV. Measurements were performed considering three  $p_{\text{T}}$  thresholds for associated charged particles:  $p_{\text{T}} > 0.15$  GeV/c,  $p_{\text{T}} > 0.5$  GeV/c, and  $p_{\text{T}} > 1$  GeV/c. Data are compared with PYTHIA 8 and EPOS LHC predictions. The coloured boxes and the error bars represent the systematic and statistical uncertainties, respectively.

## 4 Results and discussion

### 4.1 Underlying-event observables: pp compared to p–Pb collisions

Figure 2 compares the charged-particle number density as a function of  $p_{\text{T}}^{\text{trig}}$  in the transverse region for the three  $p_{\text{T}}$  thresholds: 0.15 GeV/c, 0.5 GeV/c, and 1 GeV/c. The results from pp and p–Pb collisions exhibit similar behaviour: the number density steeply rises for low  $p_{\text{T}}^{\text{trig}}$ , and it flattens at  $p_{\text{T}}^{\text{trig}} \approx 5$  GeV/c (plateau region). In the plateau region, the event activity in p–Pb collisions is  $\approx 2$  times larger than the one measured in pp collisions. This increase is smaller than that (about a factor of 3) observed for the charged-particle multiplicity densities  $dN_{\text{ch}}/d\eta$  in non-single-diffractive p–Pb collisions compared to pp collisions at the same nucleon–nucleon centre-of-mass energy [46]. It should also be noted that for both collision systems increasing the  $p_{\text{T}}$  threshold from 0.15 GeV/c to 1.0 GeV/c reduces the charged-particle number density by about a factor of 4. For pp collisions, the charged-particle number density shows a slightly increasing trend with increasing  $p_{\text{T}}^{\text{trig}}$  in the plateau region ( $p_{\text{T}}^{\text{trig}} > 5$  GeV/c). This increase is more pronounced for larger values of the  $p_{\text{T}}$  threshold for associated tracks, indicating an increased contribution of correlated hard processes (initial- and final-state radiation) to the transverse region. For example, for the  $p_{\text{T}}$  threshold  $p_{\text{T}} > 1$  GeV/c, the charged-particle number density increases from 0.3 to 0.45 (i.e., by about 50%) when  $p_{\text{T}}^{\text{trig}}$  is increased from 5 to 40 GeV/c. Whereas for the  $p_{\text{T}}$  threshold  $p_{\text{T}} > 0.15$  GeV/c, the increase is less than 10%. In contrast, for p–Pb collisions the charged-particle number density in the plateau region is flat for all the  $p_{\text{T}}$  thresholds. This behaviour also suggests that the contamination from the main partonic scattering in the transverse region is smaller in p–Pb than in pp collisions. Figure 2 also shows the predictions of the event generators. EPOS LHC better describes the  $p_{\text{T}}^{\text{trig}}$  dependence of the charged-particle multiplicity density for pp collisions relative to p–Pb collisions. However, at  $p_{\text{T}}^{\text{trig}} \approx 3$  GeV/c, the EPOS LHC predictions for pp collisions exhibit a bump that is not seen in the data and is not present in the PYTHIA 8/Monash results. For p–Pb collisions, EPOS LHC significantly underestimates the charged-particle number density, and it does not reproduce the trend with  $p_{\text{T}}^{\text{trig}}$  and the value at the plateau observed in data. In contrast, PYTHIA 8/Angantyr qualitatively reproduces the measured trends with  $p_{\text{T}}^{\text{trig}}$  in p–Pb collisions, providing a good quantitative description of the data for the lowest  $p_{\text{T}}$  threshold ( $p_{\text{T}} > 0.15$  GeV/c), while it underestimates the measured densities in the



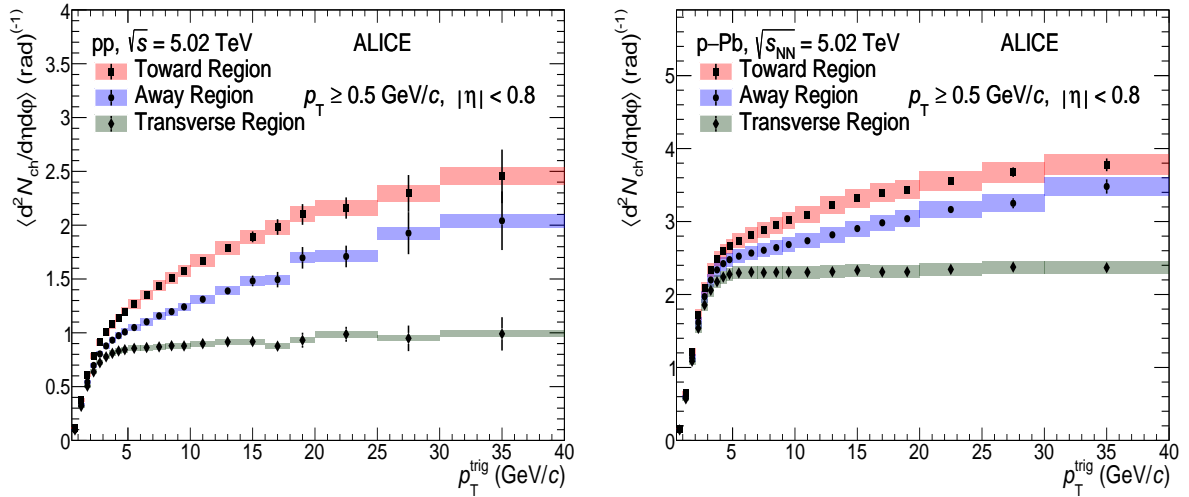
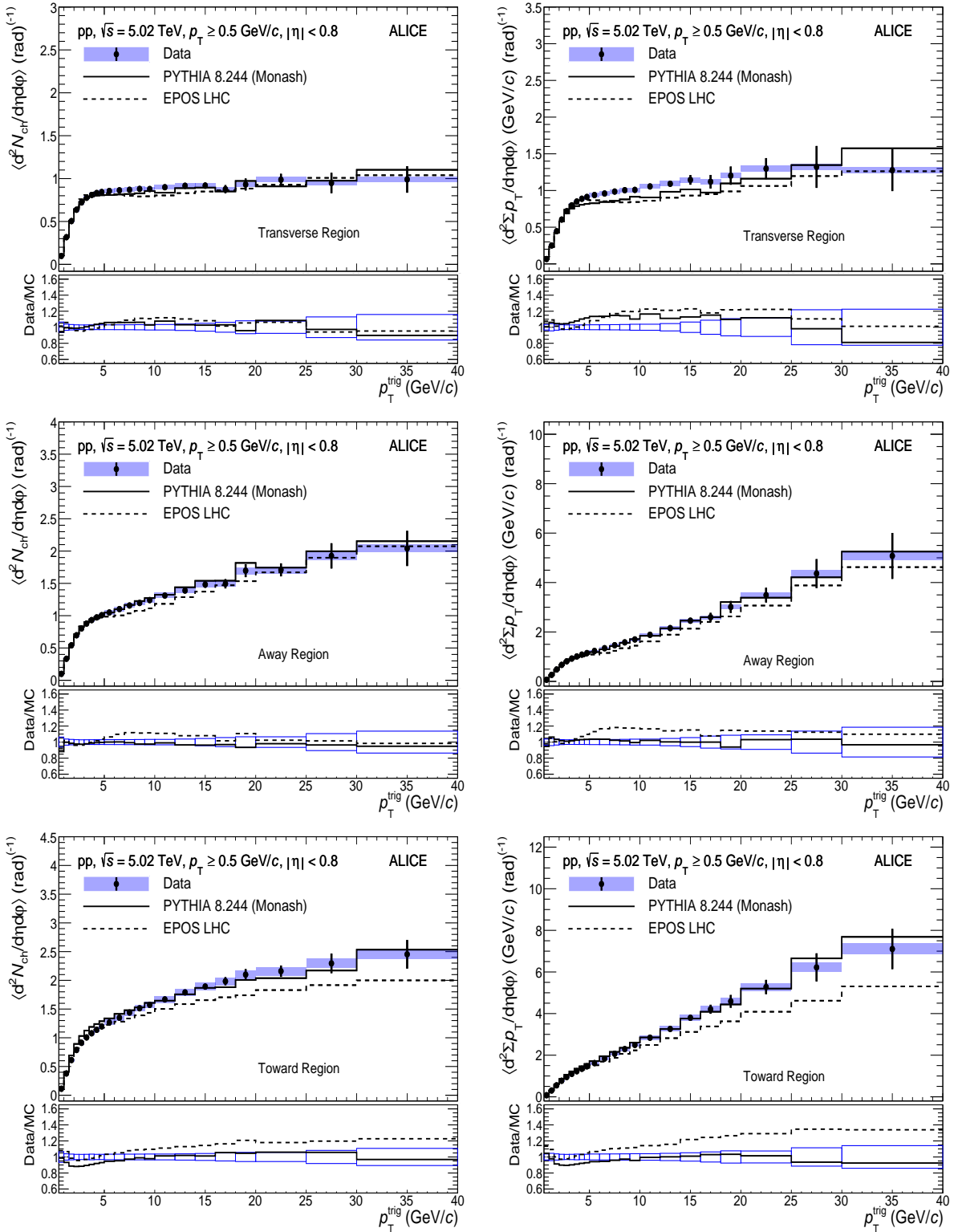


**Figure 3:** Charged-particle number density as a function of  $p_T^{\text{trig}}$  measured in pp (left) and p–Pb collisions (right) at  $\sqrt{s_{\text{NN}}} = 5.02$  TeV. Measurements were performed considering associated charged particles with  $p_T > 0.5$  GeV/c. Results for the toward, transverse, and away regions are displayed. The coloured boxes and the error bars represent the systematic and statistical uncertainties, respectively.

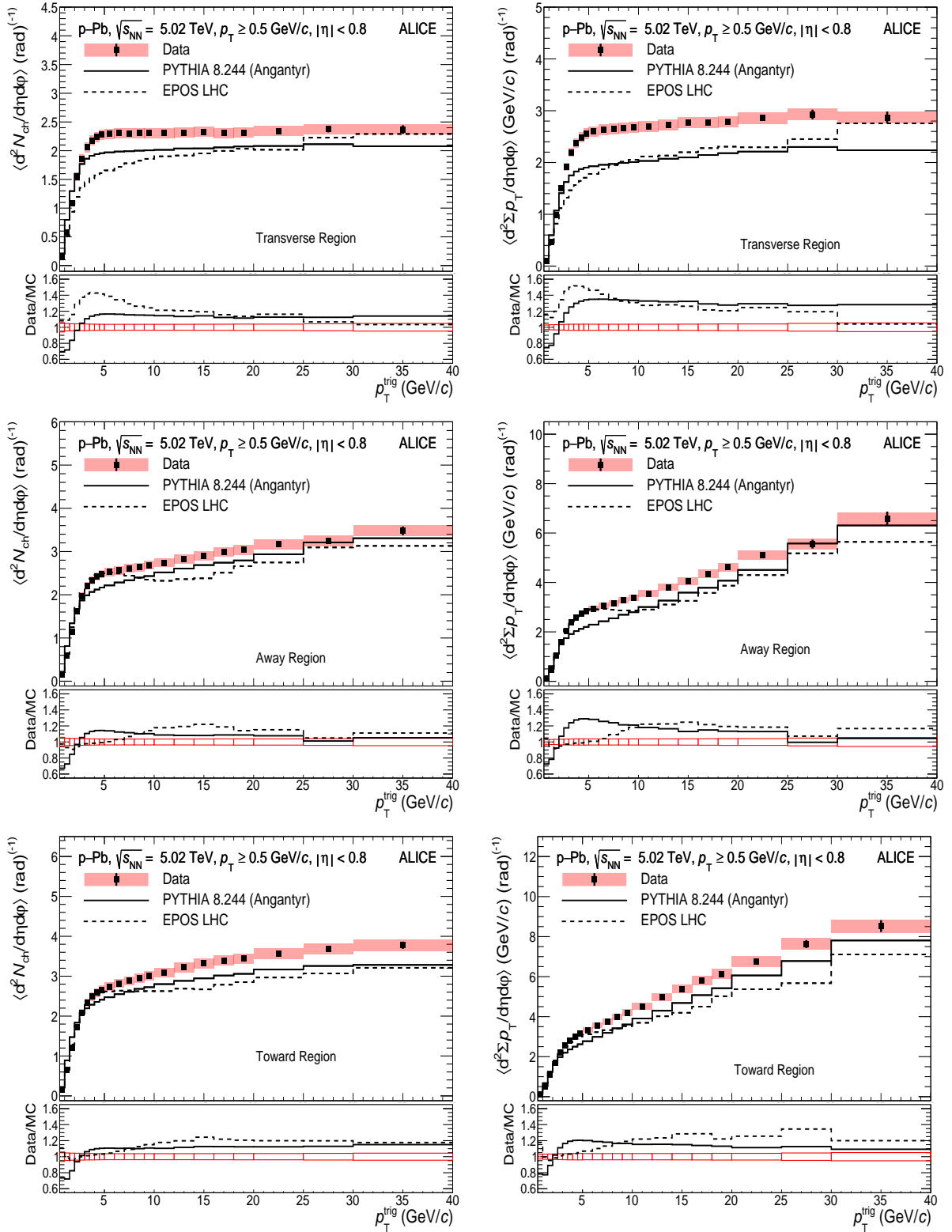
plateau region for higher  $p_T$  thresholds. In the following, measurements with the  $p_T$  threshold requirement of 0.5 GeV/c for associated particles are reported and discussed. Results for other  $p_T$  thresholds ( $p_T > 0.15$  GeV/c and  $> 1.0$  GeV/c) are presented in Appendix A.

Figure 3 shows the charged-particle number density as a function of  $p_T^{\text{trig}}$  measured in pp and p–Pb collisions at  $\sqrt{s_{\text{NN}}} = 5.02$  TeV. Results are presented for the toward, transverse, and away regions. The  $p_T^{\text{trig}}$  dependence in all regions is similar for both collision systems. For  $p_T^{\text{trig}} \gtrsim 5$  GeV/c the charged-particle number density becomes almost independent of  $p_T^{\text{trig}}$  (plateau) in the transverse region, as already pointed out above, while in the toward and away regions it continues to rise with increasing  $p_T^{\text{trig}}$ . The continuous rise observed for the toward and away regions can be attributed to the fact that produced particles in these regions do not originate only from the UE, but have also a contribution due to fragments from hard scatterings, which are mostly collimated in azimuth. The contribution from fragments increases with increasing  $p_T^{\text{trig}}$  causing the rise of event activity. A qualitatively similar behaviour in pp and p–Pb collisions is observed. However, the event activity in the toward and away regions in pp collisions increases faster with  $p_T^{\text{trig}}$  than in p–Pb collisions, namely, the increase of the particle density from  $p_T^{\text{trig}} = 5$  GeV/c up to  $p_T^{\text{trig}} = 40$  GeV/c amounts to a factor of  $\approx 2$  and  $\approx 1.4$  in pp and p–Pb collisions, respectively. Moreover, at  $p_T^{\text{trig}} = 35$  GeV/c the relative level of the event activity in the transverse region with respect to that in the toward (away) region is  $\approx 0.4$  and  $\approx 0.60$  ( $\approx 0.5$  and  $\approx 0.65$ ) for pp and p–Pb collisions, respectively. This indicates that the UE contribution to the toward and away regions is larger in p–Pb than in pp collisions, which is expected because of multiple nucleon–nucleon collisions in a single p–Pb collision that give a large additional UE, with respect to MPI in the same pp collision.

Figure 4 shows comparisons between the data from pp collisions and the predictions of event generators for both the primary charged-particle number, and the summed- $p_T$  densities in the three considered azimuthal regions (toward, away, and transverse). Although the modelling of the UE activity in PYTHIA 8/Monash is completely different with respect to that implemented in EPOS LHC, both models qualitatively describe the measured charged-particle densities in the three azimuthal regions. In the away region, within uncertainties, PYTHIA 8/Monash describes the data better than EPOS LHC in the full  $p_T^{\text{trig}}$  range of the measurement. The maximum deviation of EPOS LHC with respect to data is around 10%



**Figure 4:** The charged-particle number (left) and summed- $p_T$  (right) densities as a function of  $p_T^{trig}$  in pp collisions at  $\sqrt{s} = 5.02$  TeV are displayed. Results for the transverse (top), away (middle), and toward (bottom) regions were obtained for the transverse momentum threshold  $p_T > 0.5$  GeV/c. The shaded area and the error bars around the data points represent the systematic and statistical uncertainties, respectively. Data are compared with PYTHIA 8/Monash (solid line) and EPOS LHC (dashed line) predictions. The data-to-model ratios are displayed in the bottom panel of each plot. The boxes around unity represent the statistical and systematic uncertainties added in quadrature.



**Figure 5:** The charged-particle number (left) and summed- $p_T$  (right) densities as a function of  $p_T^{trig}$  in p-Pb collisions at  $\sqrt{s_{NN}} = 5.02$  TeV are displayed. Results for the transverse (top), away (middle), and toward (bottom) regions were obtained for the transverse momentum threshold  $p_T > 0.5$  GeV/c. The shaded area and the error bars around the data points represent the systematic and statistical uncertainties, respectively. Data are compared with PYTHIA 8/Angantyr (solid line) and EPOS LHC (dashed line) predictions. The data-to-model ratios are displayed in the bottom panel of each plot. The boxes around unity represent the statistical and systematic uncertainties added in quadrature.

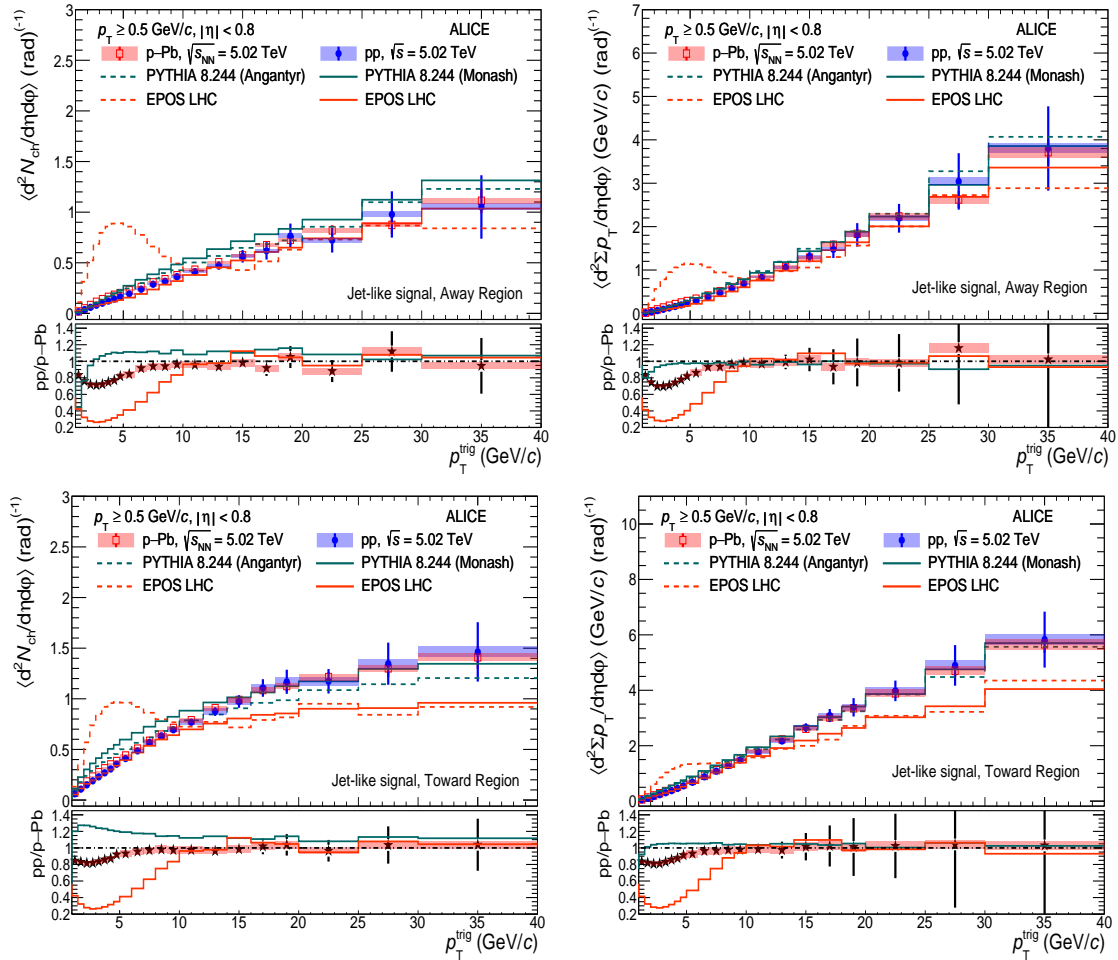


**Figure 6:** Upper panels: charged-particle number (left) and summed- $p_T$  (right) densities as a function of  $p_T^{\text{trig}}$  in pp (blue) and p–Pb (red) collisions at  $\sqrt{s_{NN}} = 5.02$  TeV. Results for data and comparison with models PYTHIA 8 (green) and EPOS LHC (red) predictions for the away (upper) and toward (bottom) regions, after the subtraction of the charged-particle number (left) and summed- $p_T$  (right) densities in the transverse region, are shown. Bottom panels: charged-particle number and summed- $p_T$  densities measured in pp collisions divided by those in p–Pb collisions are displayed for both data and models.

and 20% for the number density and summed- $p_T$  density, respectively, in the  $p_T^{\text{trig}}$  interval 5–15 GeV/c. Regarding the toward region, PYTHIA 8/Monash predictions overestimate the event activity by 10% for  $p_T^{\text{trig}} < 5$  GeV/c, whereas for higher  $p_T^{\text{trig}}$  PYTHIA 8/Monash describes the data quite well. The situation is the opposite for EPOS LHC: at low  $p_T^{\text{trig}}$  EPOS LHC describes well the event activity, but it significantly underestimates the particle densities for higher  $p_T^{\text{trig}}$  ( $> 8$  GeV/c) by  $\approx 30\%$ .

Figure 5 shows data-to-model comparisons for the case of p–Pb collisions. For the transverse region, as already pointed out above, PYTHIA 8/Angantyr provides a better qualitative description of the measured trend of the charged-particle number densities as compared to EPOS LHC. However, both PYTHIA 8/Angantyr and EPOS LHC underestimate the charged-particle summed- $p_T$  (number) density for  $p_T^{\text{trig}} > 5$  GeV/c by more than 20% (10%). While for PYTHIA 8/Angantyr this discrepancy stays roughly constant up to  $p_T \approx 3$  GeV/c, for EPOS LHC the discrepancy increases up to 50% at  $p_T \approx 3$  GeV/c. For the toward and away regions, as visible from the ratio plots in the bottom panels of Fig. 5, PYTHIA 8/Angantyr does not describe the trend with  $p_T^{\text{trig}}$  of both the event-activity variables, in particular in the range  $1 < p_T^{\text{trig}} < 5$  GeV/c, where the event activity increases more steeply in the data

than in the PYTHIA 8/Angantyr predictions. At higher  $p_{\text{T}}^{\text{trig}}$  ( $5 < p_{\text{T}}^{\text{trig}} < 10$  GeV/ $c$ ) the ratio between the data and PYTHIA 8/Angantyr flattens, however a discrepancy by about 10% (30%) between the data and the model predictions is observed for the charged-particle number (summed- $p_{\text{T}}$ ) densities. The description of the data by EPOS LHC is slightly better than that of PYTHIA 8/Angantyr for  $p_{\text{T}}^{\text{trig}} < 8$  GeV/ $c$ . However, in that  $p_{\text{T}}^{\text{trig}}$  interval EPOS LHC predicts bump structures in the toward and away regions which are not seen in data. For higher  $p_{\text{T}}^{\text{trig}}$  EPOS LHC overestimates the event activity. The inclusion of these data in future MC tunings would be relevant to improve the modelling of the UE in p–Pb collisions.

## 4.2 Event activity in the jet-like signals

Figure 6 shows the jet-like contribution to the charged-particle number and summed- $p_{\text{T}}$  densities in the toward and away regions as a function of  $p_{\text{T}}^{\text{trig}}$  for pp and p–Pb collisions at  $\sqrt{s_{\text{NN}}} = 5.02$  TeV. As discussed earlier, the event activity for the jet-like signals is obtained from the event activity in the toward and away regions after subtracting the event activity in the transverse region (see Eq. 3 and Eq. 4). In contrast to the behaviour observed for the toward and away regions, where at  $p_{\text{T}}^{\text{trig}} \approx 5$  GeV/ $c$  the event activity tends to flatten out, the densities in the jet-like signals rise with increasing  $p_{\text{T}}^{\text{trig}}$  in the entire range of the measurement.

At high  $p_{\text{T}}^{\text{trig}}$  ( $p_{\text{T}}^{\text{trig}} > 10$  GeV/ $c$ ), the event activity in the jet-like signals exhibits a remarkable similarity between measurements in pp and p–Pb collisions for both charged-particle multiplicity and summed- $p_{\text{T}}$  densities. Within 10%, both PYTHIA 8/Angantyr and EPOS LHC reproduce this feature. At low  $p_{\text{T}}^{\text{trig}}$  ( $p_{\text{T}}^{\text{trig}} < 10$  GeV/ $c$ ), the models overestimate the event activity in the jet-like signals measured in p–Pb collisions. The disagreement is more remarkable for EPOS LHC than for PYTHIA 8/Angantyr. For pp collisions, PYTHIA 8 slightly overestimates the event activity, while EPOS LHC underestimates the particle densities. For  $p_{\text{T}}^{\text{trig}} < 10$  GeV/ $c$ , the event activity in pp collisions scaled to that in p–Pb collisions is smaller than unity, reaching a minimum of  $\approx 0.8$  at  $p_{\text{T}}^{\text{trig}} \approx 3$  GeV/ $c$ . This behaviour is not reproduced by PYTHIA 8/Angantyr, which gives a ratio above unity for  $p_{\text{T}}^{\text{trig}} > 1$  GeV/ $c$ . In contrast, EPOS LHC exhibits a similar pattern, but the size of the effect is much larger than in data. The main difference between PYTHIA 8/Angantyr and EPOS LHC is that EPOS LHC incorporates collective flow, which is expected to be significant in the  $p_{\text{T}}^{\text{trig}}$  interval where we observe the differences between measurements in pp and p–Pb collisions. Given that (radial and elliptic) flow is larger in p–Pb than in pp collisions [47, 48], its contribution to the toward and away regions is expected to be higher in p–Pb than in pp collisions. In particular, the elliptic azimuthal correlations modulate the background according to:  $B(\Delta\phi) = B_0 \left( 1 + 2V_2 \cos(2\Delta\phi) \right)$ , where  $V_2 \approx v_2^{\text{trig}} v_2^{\text{assoc}}$  is approximately given by the product of anisotropic flow coefficients for trigger and associated particles at their respective momenta [49]. From Pb–Pb results we expect the effect to be the largest at intermediate transverse momenta and to decrease for high transverse momentum particles [50].

Finally, the average transverse momentum  $\langle p_{\text{T}} \rangle$  of particles in the toward and away regions after subtracting the UE contribution estimated from the transverse region is shown in Fig. 7 as a function of  $p_{\text{T}}^{\text{trig}}$  for pp and p–Pb collisions at  $\sqrt{s_{\text{NN}}} = 5.02$  TeV. Within uncertainties, the  $\langle p_{\text{T}} \rangle$  values are consistent in pp and p–Pb collisions in the measured  $p_{\text{T}}^{\text{trig}}$  interval. The PYTHIA 8 tunes considered in this paper do not reproduce this behaviour. They predict that in the away region the average  $p_{\text{T}}$  for the jet-like signal in pp collisions is about 20% (10%) larger than in p–Pb collisions for  $p_{\text{T}}^{\text{trig}} < 2$  GeV/ $c$  ( $p_{\text{T}}^{\text{trig}} > 5$  GeV/ $c$ ). For the toward region, the situation is similar at high  $p_{\text{T}}^{\text{trig}}$ ; however, for  $p_{\text{T}}^{\text{trig}} < 2$  GeV/ $c$ , the  $\langle p_{\text{T}} \rangle$  in p–Pb collisions is predicted to be about 20% larger than in pp collisions. Although the main source of this discrepancy is the underestimation of the measured  $\langle p_{\text{T}} \rangle$  in p–Pb collisions by PYTHIA 8/Angantyr, the prediction for pp collisions is lower than the measured  $\langle p_{\text{T}} \rangle$  in the away region. The agreement of PYTHIA 8/Monash with pp data is better for the toward region. On the other hand, EPOS LHC reproduces the average  $p_{\text{T}}$  for the two collision systems better than PYTHIA 8/Angantyr. Although,

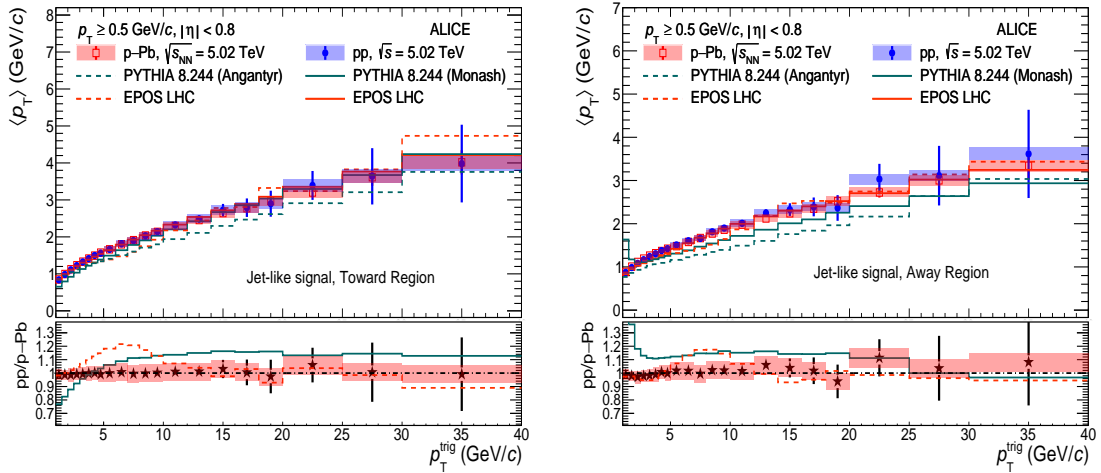


**Figure 7:** Upper: average transverse momentum as a function of  $p_T^{\text{trig}}$  in the toward (left) and away (right) regions measured in pp and p–Pb collisions at  $\sqrt{s_{NN}} = 5.02$  TeV. Results for data and comparison with models PYTHIA 8 (green) and EPOS LHC (red) predictions are shown. Bottom: average transverse momentum measured in pp collisions divided by that measured in p–Pb collisions. A similar ratio is shown for model predictions.

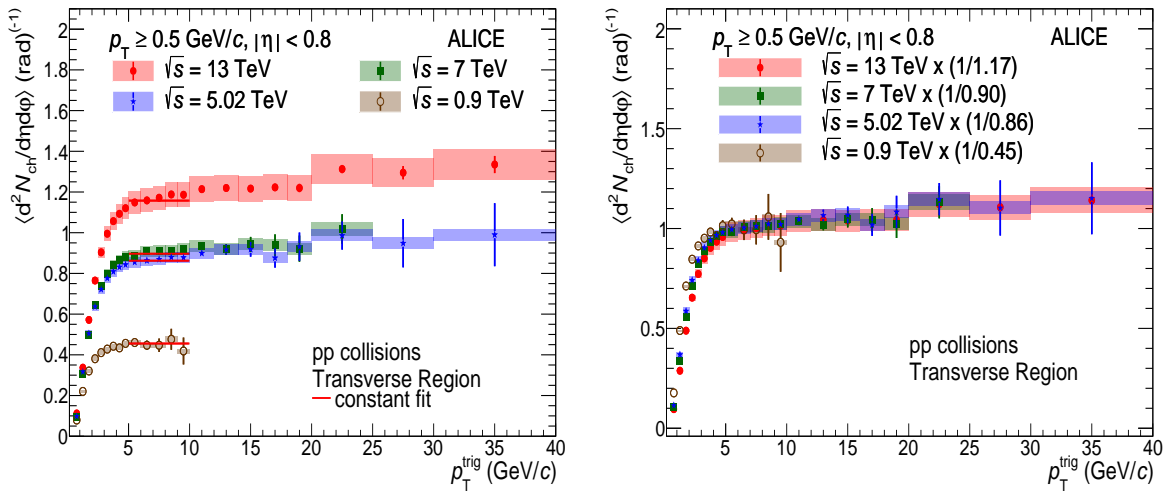


**Figure 8:** Left: charged-particle number density in the transverse region as a function of  $p_T^{\text{trig}}$  for pp collisions at  $\sqrt{s} = 0.9, 5.02, 7, 13$  TeV [11, 14]. A constant function (solid lines) is used to fit the data in the range  $5 < p_T^{\text{trig}} < 10$  GeV/c. Right: number densities scaled by the plateau values obtained from the fit to compare the shapes. The coloured boxes represent the systematic uncertainties, and vertical error bars indicate statistical uncertainties.

for  $p_T^{\text{trig}} < 10$  GeV/c, EPOS LHC predicts the  $\langle p_T \rangle$  in the toward region to be larger in pp as compared to p–Pb collisions, leading to a bump-like structure in the ratio of pp over p–Pb results, which is not observed in the data.

### 4.3 Energy dependence of the underlying event in pp collisions

This subsection discusses the collision-energy dependence of the charged-particle number density in the transverse region. Given that data from experiments at RHIC, the Tevatron and the LHC, are available for the  $p_T$  threshold,  $p_T > 0.5$  GeV/c, our results for this  $p_T$  threshold are compared with existing measure-

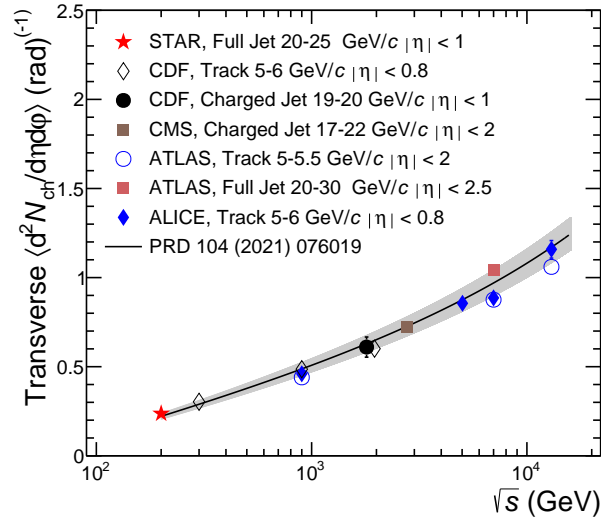


**Figure 9:** Centre-of-mass energy dependence of the high  $p_{\text{T}}^{\text{trig}}$  plateau value of the charged-particle number density in the transverse region. The ATLAS [53–55], CDF [2, 56], CMS [57] and STAR [3] data points were taken from the compilation reported by the STAR collaboration [3]. Error bars represent statistical and systematic uncertainties summed in quadrature. The data are compared with a parametrisation of the form  $s^{0.27} + 0.14 \log(s)$  [58].

ments at other centre-of-mass energies. Figure 8 (left) compares the UE activity obtained in pp collisions at  $\sqrt{s} = 5.02$  TeV to those obtained at other LHC energies, namely  $\sqrt{s} = 0.9, 7,$  and  $13$  TeV [11, 14]. Between the two higher energies,  $\sqrt{s} = 7$  and  $13$  TeV, the number density in the plateau increases by about 30%. A similar increase was reported considering associated particles with  $p_{\text{T}} > 0.15$  GeV/c [51]. More information about the  $\sqrt{s}$ -dependence in the transverse region can be obtained by comparing the shapes of the number density as a function of  $p_{\text{T}}^{\text{trig}}$ . One attempt using the data provided by the ATLAS collaboration has been reported in Ref. [52]; a similar comparison was performed by the ALICE collaboration in Ref. [51]. Following the approach presented in Ref. [51], the height of the plateau for different collision energies is quantified by fitting a constant function in the range  $5 < p_{\text{T}}^{\text{trig}} < 10$  GeV/c (the fit functions are also shown in the left panel of Fig. 8). The fitting range was restricted to that common range in order to be consistent with the procedure used for the measurements at other centre-of-mass energies. Larger fitting ranges were also considered, and consistent results were obtained. The shapes of the particle densities as a function of  $p_{\text{T}}^{\text{trig}}$  are then compared after dividing the densities by the level of the plateau, as estimated from the fit to a constant value. The results are shown in Fig. 8 (right). For the two higher energies, the  $p_{\text{T}}^{\text{trig}}$  coverage extends beyond the fitting range, i.e. to  $p_{\text{T}}^{\text{trig}} > 10$  GeV/c. In this range, the densities agree within the statistical and systematic uncertainties. In the rise region ( $p_{\text{T}}^{\text{trig}} < 5$  GeV/c), one observes a clear ordering among the four collision energies, the lowest energy having the highest density relative to the plateau. Moreover, at lower  $\sqrt{s}$ , the plateau values seem to be reached at a slightly lower  $p_{\text{T}}^{\text{trig}}$ . This feature is also observed in pp collisions simulated with the PYTHIA 8 event generator [52].

Figure 9 shows the  $\sqrt{s}$  dependence of the charged-particle number density measured in the transverse azimuthal interval and in the high  $p_{\text{T}}^{\text{trig}}$  interval of the plateau region. Results from various experiments at RHIC [3], the Tevatron [2, 56], and the LHC [11, 51, 53–55, 57] are displayed. The ATLAS, CDF, CMS, and STAR data points are taken from the compilation reported by the STAR collaboration [3]. The event activity shows a modest increase from  $\sqrt{s} = 0.2$  up to  $0.9$  TeV, while for higher energies it exhibits a steeper rise. This behaviour is described by a function of the form  $\propto s^{0.27} + 0.14 \log(s)$ , in which the power-law term describes the UE contribution, whereas the logarithmic term describes the contribution from ISR and FSR. The parametrisation was taken from Ref. [58]. A comparison to the charged particle multiplicity at mid-pseudorapidity in minimum-bias pp data, where  $dN_{\text{ch}}/d\eta$  can be parameterised as  $dN_{\text{ch}}/d\eta \propto s^{0.114}$  [59], suggests that the UE contribution increases faster with centre-of-mass energy

than the charged particle multiplicity in minimum-bias pp collisions.

## 5 Conclusions

In this paper, the measurements of underlying-event observables performed in pp and p–Pb collisions at a centre-of-mass energy per nucleon–nucleon collisions of 5.02 TeV were reported. The analysis was carried out following the strategy introduced by the CDF collaboration consisting of the definition of three azimuthal regions relative to the highest transverse momentum particle in the collision ( $p_{\text{T}}^{\text{trig}}$ ). The charged-particle production is measured within the pseudorapidity interval  $|\eta| < 0.8$ ; and it is quantified with the number and summed- $p_{\text{T}}$  densities considering particles above a given  $p_{\text{T}}$  threshold. Three  $p_{\text{T}}$  thresholds are considered: 0.15, 0.5, and 1 GeV/ $c$ . These quantities are reported as a function of  $p_{\text{T}}^{\text{trig}}$ , and for the toward, away, and transverse azimuthal regions. The transverse region is the most sensitive to the underlying event; while the toward and away regions include both the underlying-event and jet fragments from the main partonic scattering. For the isolation of the jet-like signal, the event activity in the transverse region is subtracted from those measured in the toward and away regions. Results for pp collisions are compared with data at other centre-of-mass energies and with MC predictions. In addition, the event activities measured in pp and p–Pb collisions are compared with each other at the same  $p_{\text{T}}^{\text{trig}}$  value. The main conclusions of the present work are listed below.

- The underlying-event observables in pp collisions follow the same behaviour as observed at lower centre-of-mass energies. In the transverse region the charged-particle densities measured in the three azimuthal regions exhibit a fast rise for  $p_{\text{T}}^{\text{trig}} < 5$  GeV/ $c$  followed by a flattening at higher  $p_{\text{T}}^{\text{trig}}$  (plateau). Data for the three azimuthal regions relative to the leading particle are reproduced by the PYTHIA 8 event generator with the Monash tune. EPOS LHC predicts a slightly different behaviour in particular at  $p_{\text{T}}^{\text{trig}}$  around 3 GeV/ $c$  where a bump structure is present in the three azimuthal regions which is not observed in the data.
- The underlying-event observables in p–Pb collisions qualitatively behave like in pp interactions. The particle densities in the transverse region exhibit a saturation at  $p_{\text{T}}^{\text{trig}} \approx 5$  GeV/ $c$ . PYTHIA 8/Angantyr qualitatively reproduces this saturation but underestimates the particle densities. The EPOS LHC model does not describe the saturation and underestimates the event activity within the measured  $p_{\text{T}}^{\text{trig}}$  interval. For the toward and away regions, above the onset of the plateau, data exhibit a slower increase of the particle densities with increasing  $p_{\text{T}}^{\text{trig}}$  than that observed in pp collisions. EPOS LHC and PYTHIA 8/Angantyr underestimate the particle densities at high  $p_{\text{T}}^{\text{trig}}$  ( $> 8$  GeV/ $c$ ). At lower  $p_{\text{T}}^{\text{trig}}$ , EPOS LHC predicts a bump structure at  $p_{\text{T}}^{\text{trig}} \approx 4$  GeV/ $c$  which is not seen in data. For  $p_{\text{T}}^{\text{trig}} < 3$  GeV/ $c$ , EPOS LHC describes the particle densities, whereas PYTHIA 8/Angantyr overestimates those in data by up to 30%.
- The particle densities in the toward and away regions after subtraction of the UE contribution as a function of  $p_{\text{T}}^{\text{trig}}$  in pp collisions are consistent with those measured in p–Pb collisions for  $p_{\text{T}}^{\text{trig}} > 10$  GeV/ $c$ , i.e., no modification of the jet-like yield in p–Pb collisions relative to pp collisions is found. At lower  $p_{\text{T}}^{\text{trig}}$ , the charged-particle densities are larger in p–Pb collisions relative to pp collisions. This behaviour is expected given the larger collective flow effects in p–Pb collisions relative to pp collisions. This feature is qualitatively captured by the EPOS LHC generator, which incorporates collective flow effects in the modelling of the system created in the collision. However, the size of the effect is significantly larger in EPOS LHC than in data. An opposite trend is instead predicted by simulations with PYTHIA 8/Angantyr, which do not include collective effects. The average  $p_{\text{T}}$  as a function of  $p_{\text{T}}^{\text{trig}}$  was also measured. The average  $p_{\text{T}}$  values measured in pp and p–Pb collision are found to be consistent between each other in the entire  $p_{\text{T}}^{\text{trig}}$  interval of



the measurement. Simulations with EPOS LHC predict instead a slightly lower average  $p_T$  for jet-like signal in p–Pb collisions as compared to pp collisions for  $p_T^{\text{trig}} < 10$  GeV/c, while PYTHIA 8 with the Monash and Angantyr tunes do not provide a good description for this observable.

The measurements reported in this article represent important input for the tuning of some of the parameters of the event generators in order to improve the modelling of soft particle production in pp and p–Pb collisions. Moreover, they can contribute to the understanding of the origin of signals resembling a collective behaviour in pp and p–Pb collisions.

## References

- [1] T. Sjöstrand and M. van Zijl, “A Multiple Interaction Model for the Event Structure in Hadron Collisions”, *Phys. Rev. D* **36** no. 2019, (1987) .
- [2] **CDF** Collaboration, T. Affolder *et al.*, “Charged Jet Evolution and the Underlying Event in  $p\bar{p}$  Collisions at 1.8 TeV”, *Phys. Rev. D* **65** no. 092002, (2002) .
- [3] **STAR** Collaboration, J. Adam *et al.*, “Underlying event measurements in  $p + p$  collisions at  $\sqrt{s} = 200$  GeV at RHIC”, *Phys. Rev. D* **101** no. 052004, (2020) , arXiv:1912.08187 [nucl-ex].
- [4] C. M. Buttar *et al.*, “The Underlying Event”, in *HERA and the LHC: A Workshop on the Implications of HERA for LHC Physics: CERN - DESY Workshop 2004/2005 (Midterm Meeting, CERN, 11-13 October 2004; Final Meeting, DESY, 17-21 January 2005)*. CERN, Geneva, 12, 2005.
- [5] **STAR** Collaboration, J. Adam *et al.*, “Underlying event measurements in  $p + p$  collisions at  $\sqrt{s} = 200$  GeV at RHIC”, *Phys. Rev. D* **101** no. 052004, (2020) , arXiv:1912.08187 [nucl-ex].
- [6] **CDF** Collaboration, D. Acosta *et al.*, “The underlying event in hard interactions at the Tevatron  $\bar{p}p$  collider”, *Phys. Rev. D* **70** no. 072002, (2004) , arXiv:hep-ex/0404004.
- [7] R. Field, “Min-Bias and the Underlying Event at the LHC”, *Acta Phys. Polon. B* **42** no. 2631, (2011) , arXiv:1110.5530 [hep-ph].
- [8] **CDF** Collaboration, T. Aaltonen *et al.*, “Studying the Underlying Event in Drell-Yan and High Transverse Momentum Jet Production at the Tevatron”, *Phys. Rev. D* **82** no. 034001, (2010) , arXiv:1003.3146 [hep-ex].
- [9] **CMS** Collaboration, V. Khachatryan *et al.*, “First Measurement of the Underlying Event Activity at the LHC with  $\sqrt{s} = 0.9$  TeV”, *Eur. Phys. J. C* **70** no. 555, (2010) , arXiv:1006.2083 [hep-ex].
- [10] **ATLAS** Collaboration, G. Aad *et al.*, “Measurement of underlying event characteristics using charged particles in pp collisions at  $\sqrt{s} = 900$  GeV and 7 TeV with the ATLAS detector”, *Phys. Rev. D* **83** no. 112001, (2011) , arXiv:1012.0791 [hep-ex].
- [11] **ALICE** Collaboration, B. Abelev *et al.*, “Underlying Event measurements in pp collisions at  $\sqrt{s} = 0.9$  and 7 TeV with the ALICE experiment at the LHC”, *JHEP* **07** no. 116, (2012) , arXiv:1112.2082 [hep-ex].
- [12] **ATLAS** Collaboration, G. Aad *et al.*, “Measurement of the underlying event in jet events from 7 TeV proton-proton collisions with the ATLAS detector”, *Eur. Phys. J. C* **74** no. 8, (2014) , arXiv:1406.0392 [hep-ex].

- [13] **ATLAS** Collaboration, M. Aaboud *et al.*, “Measurement of charged-particle distributions sensitive to the underlying event in  $\sqrt{s} = 13$  TeV proton-proton collisions with the ATLAS detector at the LHC”, *JHEP* **03** no. 157, (2017), arXiv:1701.05390 [hep-ex].
- [14] **ALICE** Collaboration, S. Acharya *et al.*, “Underlying Event properties in pp collisions at  $\sqrt{s} = 13$  TeV”, *JHEP* **04** no. 192, (2020), arXiv:1910.14400 [nucl-ex].
- [15] **CMS** Collaboration, S. Chatrchyan *et al.*, “Measurement of the underlying event in the Drell-Yan process in proton-proton collisions at  $\sqrt{s} = 7$  TeV”, *Eur. Phys. J. C* **72** no. 2080, (2012), arXiv:1204.1411 [hep-ex].
- [16] **ATLAS** Collaboration, G. Aad *et al.*, “Measurement of distributions sensitive to the underlying event in inclusive Z-boson production in pp collisions at  $\sqrt{s} = 7$  TeV with the ATLAS detector”, *Eur. Phys. J. C* **74** no. 12, (2014), arXiv:1409.3433 [hep-ex].
- [17] **CMS** Collaboration, A. M. Sirunyan *et al.*, “Measurement of the underlying event activity in inclusive Z boson production in proton-proton collisions at  $\sqrt{s} = 13$  TeV”, *JHEP* **07** no. 032, (2018), arXiv:1711.04299 [hep-ex].
- [18] **ATLAS** Collaboration, G. Aad *et al.*, “Measurement of distributions sensitive to the underlying event in inclusive Z-boson production in pp collisions at  $\sqrt{s} = 13$  TeV with the ATLAS detector”, *Eur. Phys. J. C* **79** no. 8, (2019), arXiv:1905.09752 [hep-ex].
- [19] M. Strikman, “Transverse Nucleon Structure and Multiparton Interactions”, *Acta Phys. Polon. B* **42** no. 2607, (2011), arXiv:1112.3834 [hep-ph].
- [20] **ALICE** Collaboration, J. Adam *et al.*, “Centrality dependence of particle production in p-Pb collisions at  $\sqrt{s_{\text{NN}}} = 5.02$  TeV”, *Phys. Rev. C* **91** no. 064905, (2015), arXiv:1412.6828 [nucl-ex].
- [21] J. L. Nagle and W. A. Zajc, “Small System Collectivity in Relativistic Hadronic and Nuclear Collisions”, *Ann. Rev. Nucl. Part. Sci.* **68** (2018), arXiv:1801.03477 [nucl-ex].
- [22] **ALICE** Collaboration, J. Adam *et al.*, “Enhanced production of multi-strange hadrons in high-multiplicity proton-proton collisions”, *Nature Phys.* **13** no. 535, (2017), arXiv:1606.07424 [nucl-ex].
- [23] **ALICE** Collaboration, J. Adam *et al.*, “Multiplicity dependence of charged pion, kaon, and (anti)proton production at large transverse momentum in p-Pb collisions at  $\sqrt{s_{\text{NN}}} = 5.02$  TeV”, *Phys. Lett. B* **760** no. 720, (2016), arXiv:1601.03658 [nucl-ex].
- [24] **ALICE** Collaboration, S. Acharya *et al.*, “Multiplicity dependence of light-flavor hadron production in pp collisions at  $\sqrt{s} = 7$  TeV”, *Phys. Rev. C* **99** no. 2, (2019), arXiv:1807.11321 [nucl-ex].
- [25] **CMS** Collaboration, V. Khachatryan *et al.*, “Observation of Long-Range Near-Side Angular Correlations in Proton-Proton Collisions at the LHC”, *JHEP* **09** no. 091, (2010), arXiv:1009.4122 [hep-ex].
- [26] **CMS** Collaboration, V. Khachatryan *et al.*, “Evidence for collectivity in pp collisions at the LHC”, *Phys. Lett. B* **765** no. 193, (2017), arXiv:1606.06198 [nucl-ex].
- [27] T. Sjöstrand, S. Ask, J. R. Christiansen, R. Corke, N. Desai, P. Ilten, S. Mrenna, S. Prestel, C. O. Rasmussen, and P. Z. Skands, “An introduction to PYTHIA 8.2”, *Comput. Phys. Commun.* **191** (2015), arXiv:1410.3012 [hep-ph].

- [28] A. Ortiz, P. Christiansen, E. Cuautle Flores, I. Maldonado Cervantes, and G. Paic, “Color Reconnection and Flowlike Patterns in pp Collisions”, *Phys. Rev. Lett.* **111** no. 4, (2013), arXiv:1303.6326 [hep-ph].
- [29] A. Ortiz and L. Valencia Palomo, “Probing color reconnection with underlying event observables at the LHC energies”, *Phys. Rev. D* **99** no. 3, (2019), arXiv:1809.01744 [hep-ex].
- [30] P. Skands, S. Carrazza, and J. Rojo, “Tuning PYTHIA 8.1: the Monash 2013 Tune”, *Eur. Phys. J. C* **74** no. 8, (2014), arXiv:1404.5630 [hep-ph].
- [31] S. Gieseke, C. Rohr, and A. Siodmok, “Colour reconnections in Herwig++”, *Eur. Phys. J. C* **72** (2012), arXiv:1206.0041 [hep-ph].
- [32] T. Martin, P. Skands, and S. Farrington, “Probing Collective Effects in Hadronisation with the Extremes of the Underlying Event”, *Eur. Phys. J. C* **76** no. 5, (2016), arXiv:1603.05298 [hep-ph].
- [33] T. Pierog, I. Karpenko, J. M. Katzy, E. Yatsenko, and K. Werner, “EPOS LHC: Test of collective hadronization with data measured at the CERN Large Hadron Collider”, *Phys. Rev. C* **92** no. 3, (2015), arXiv:1306.0121 [hep-ph].
- [34] C. Bierlich, G. Gustafson, L. Lönnblad, and H. Shah, “The Angantyr model for Heavy-Ion Collisions in PYTHIA8”, *JHEP* **10** no. 134, (2018), arXiv:1806.10820 [hep-ph].
- [35] B. Andersson, G. Gustafson, G. Ingelman, and T. Sjöstrand, “Parton fragmentation and string dynamics”, *Physics Reports* **97** no. 2, (1983).  
<https://www.sciencedirect.com/science/article/pii/0370157383900807>.
- [36] H. Pi, “An event generator for interactions between hadrons and nuclei — fritiof version 7.0”, *Computer Physics Communications* **71** no. 1, (1992).  
<https://www.sciencedirect.com/science/article/pii/001046559290082A>.
- [37] H. J. Drescher, M. Hladik, S. Ostapchenko, T. Pierog, and K. Werner, “Parton based Gribov-Regge theory”, *Phys. Rept.* **350** (2001), arXiv:hep-ph/0007198.
- [38] ALICE Collaboration, K. Aamodt *et al.*, “The ALICE experiment at the CERN LHC”, *JINST* **3** no. 08, (2008).
- [39] ALICE Collaboration, B. B. Abelev *et al.*, “Performance of the ALICE Experiment at the CERN LHC”, *Int. J. Mod. Phys. A* **29** no. 1430044, (2014), arXiv:1402.4476 [nucl-ex].
- [40] ALICE Collaboration, “The ALICE definition of primary particles”,  
<https://cds.cern.ch/record/2270008>.
- [41] ALICE Collaboration, B. Abelev *et al.*, “Centrality Dependence of Charged Particle Production at Large Transverse Momentum in Pb–Pb Collisions at  $\sqrt{s_{NN}} = 2.76$  TeV”, *Phys. Lett. B* **720** no. 52, (2013), arXiv:1208.2711 [hep-ex].
- [42] ALICE Collaboration, S. Acharya *et al.*, “Charged-particle production as a function of multiplicity and transverse sphericity in pp collisions at  $\sqrt{s} = 5.02$  and 13 TeV”, *Eur. Phys. J. C* **79** no. 10, (2019), arXiv:1905.07208 [nucl-ex].
- [43] ALICE Collaboration, S. Acharya *et al.*, “Transverse momentum spectra and nuclear modification factors of charged particles in pp, p-Pb and Pb-Pb collisions at the LHC”, *JHEP* **11** no. 013, (2018), arXiv:1802.09145 [nucl-ex].

- [44] R. Brun, F. Bruyant, F. Carminati, S. Giani, M. Maire, A. McPherson, G. Patrick, and L. Urban, *GEANT: Detector Description and Simulation Tool; Oct 1994*. CERN Program Library. CERN, Geneva, 1993. <https://cds.cern.ch/record/1082634>. Long Writeup W5013.
- [45] ALICE Collaboration, S. Acharya *et al.*, “Production of charged pions, kaons, and (anti-)protons in Pb-Pb and inelastic pp collisions at  $\sqrt{s_{NN}} = 5.02$  TeV”, *Phys. Rev. C* **101** no. 4, (2020), arXiv:1910.07678 [nucl-ex].
- [46] CMS Collaboration, A. M. Sirunyan *et al.*, “Pseudorapidity distributions of charged hadrons in proton-lead collisions at  $\sqrt{s_{NN}} = 5.02$  and 8.16 TeV”, *JHEP* **01** no. 045, (2018), arXiv:1710.09355 [hep-ex].
- [47] ALICE Collaboration, B. B. Abelev *et al.*, “Multiplicity Dependence of Pion, Kaon, Proton and Lambda Production in p-Pb Collisions at  $\sqrt{s_{NN}} = 5.02$  TeV”, *Phys. Lett. B* **728** no. 25, (2014), arXiv:1307.6796 [nucl-ex].
- [48] ALICE Collaboration, S. Acharya *et al.*, “Investigations of Anisotropic Flow Using Multiparticle Azimuthal Correlations in pp, p-Pb, Xe-Xe, and Pb-Pb Collisions at the LHC”, *Phys. Rev. Lett.* **123** no. 142301, (2019), arXiv:1903.01790 [nucl-ex].
- [49] ALICE Collaboration, B. Abelev *et al.*, “Anisotropic flow of charged hadrons, pions and (anti-)protons measured at high transverse momentum in Pb-Pb collisions at  $\sqrt{s_{NN}}=2.76$  TeV”, *Phys. Lett. B* **719** no. 18, (2013), arXiv:1205.5761 [nucl-ex].
- [50] ALICE Collaboration, K. Aamodt *et al.*, “Particle-yield modification in jet-like azimuthal di-hadron correlations in Pb-Pb collisions at  $\sqrt{s_{NN}} = 2.76$  TeV”, *Phys. Rev. Lett.* **108** no. 092301, (2012), arXiv:1110.0121 [nucl-ex].
- [51] ALICE Collaboration, S. Acharya *et al.*, “Underlying Event properties in pp collisions at  $\sqrt{s} = 13$  TeV”, *JHEP* **04** no. 192, (2020), arXiv:1910.14400 [nucl-ex].
- [52] A. Ortiz and L. Valencia Palomo, “Universality of the underlying event in pp collisions”, *Phys. Rev. D* **96** no. 11, (2017), arXiv:1710.04741 [hep-ex].
- [53] ATLAS Collaboration, G. Aad *et al.*, “Measurement of underlying event characteristics using charged particles in pp collisions at  $\sqrt{s} = 900$  GeV and 7 TeV with the ATLAS detector”, *Phys. Rev. D* **83** (2011), arXiv:1012.0791 [hep-ex].
- [54] ATLAS Collaboration, G. Aad *et al.*, “Measurement of the underlying event in jet events from 7 TeV proton-proton collisions with the ATLAS detector”, *Eur. Phys. J. C* **74** no. 8, (2014), arXiv:1406.0392 [hep-ex].
- [55] ATLAS Collaboration, M. Aaboud *et al.*, “Measurement of charged-particle distributions sensitive to the underlying event in  $\sqrt{s} = 13$  TeV proton-proton collisions with the ATLAS detector at the LHC”, *JHEP* **03** no. 157, (2017), arXiv:1701.05390 [hep-ex].
- [56] CDF Collaboration, T. A. Aaltonen *et al.*, “Study of the energy dependence of the underlying event in proton-antiproton collisions”, *Phys. Rev. D* **92** no. 9, (2015), arXiv:1508.05340 [hep-ex].
- [57] CMS Collaboration, V. Khachatryan *et al.*, “Measurement of the underlying event activity using charged-particle jets in proton-proton collisions at  $\sqrt{s} = 2.76$  TeV”, *JHEP* **09** no. 137, (2015), arXiv:1507.07229 [hep-ex].
- [58] A. Ortiz, “Energy dependence of underlying-event observables from RHIC to LHC energies”, *Phys. Rev. D* **104** no. 076019, (2021), arXiv:2108.08360 [hep-ph].

- [59] **ALICE** Collaboration, J. Adam *et al.*, “Charged-particle multiplicities in proton–proton collisions at  $\sqrt{s} = 0.9$  to 8 TeV”, *Eur. Phys. J. C* **77** no. 1, (2017), arXiv:1509.07541 [nucl-ex].

## A Appendix

### A.1 Charged-particle densities as a function of $p_{\text{T}}^{\text{trig}}$ for others $p_{\text{T}}$ thresholds

The charged-particle number and summed- $p_{\text{T}}$  densities as a function of  $p_{\text{T}}^{\text{trig}}$  measured in pp collisions at  $\sqrt{s} = 5.02$  TeV, in the transverse, away, and toward regions for the transverse momentum thresholds  $p_{\text{T}} > 0.15$  GeV/ $c$  and  $p_{\text{T}} > 1$  GeV/ $c$  are shown in figures A.1 and A.2, respectively. The charged-particle number and summed- $p_{\text{T}}$  densities as a function of  $p_{\text{T}}^{\text{trig}}$  measured in p–Pb collisions at  $\sqrt{s_{\text{NN}}} = 5.02$  TeV, in the transverse, away, and toward regions for the transverse momentum thresholds  $p_{\text{T}} > 0.15$  GeV/ $c$  and  $p_{\text{T}} > 1$  GeV/ $c$  are shown in figures A.3 and A.4, respectively.

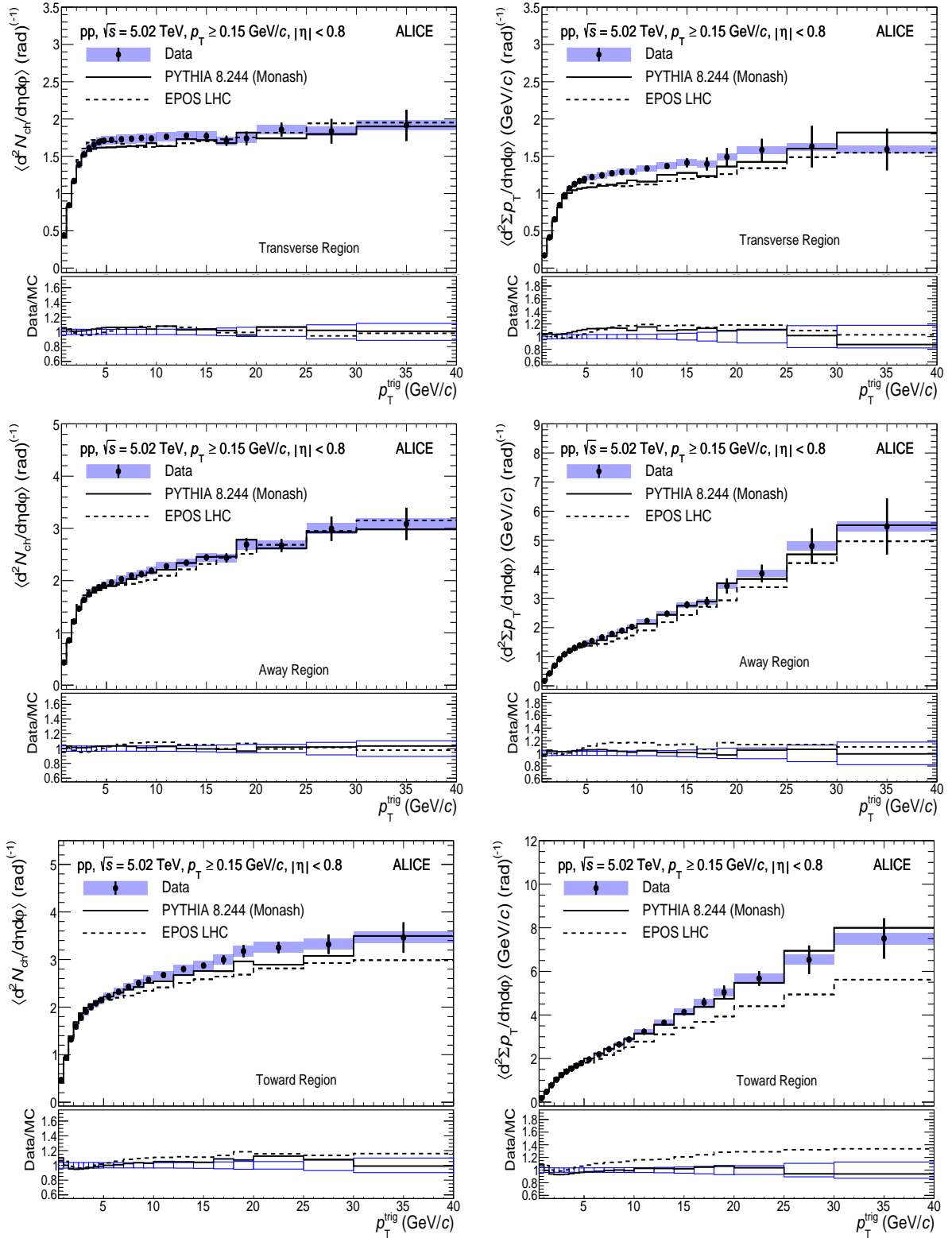


**Figure A.1:** The charged-particle number (left) and summed- $p_T$  (right) densities as a function of  $p_T^{\text{trig}}$  in pp collision at  $\sqrt{s} = 5.02$  TeV are displayed. Results for the transverse (top), away (middle), and toward (bottom) regions were obtained for the transverse momentum threshold  $p_T > 0.15$  GeV/c. The shaded area and the error bars around the data points represent the systematic and statistical uncertainties, respectively. Data are compared with PYTHIA 8/Monash (solid line) and EPOS LHC (dashed line) predictions. The data-to-model ratios are displayed in the bottom panel of each plot. The boxes around unity represent the statistical and systematic uncertainties added in quadrature.

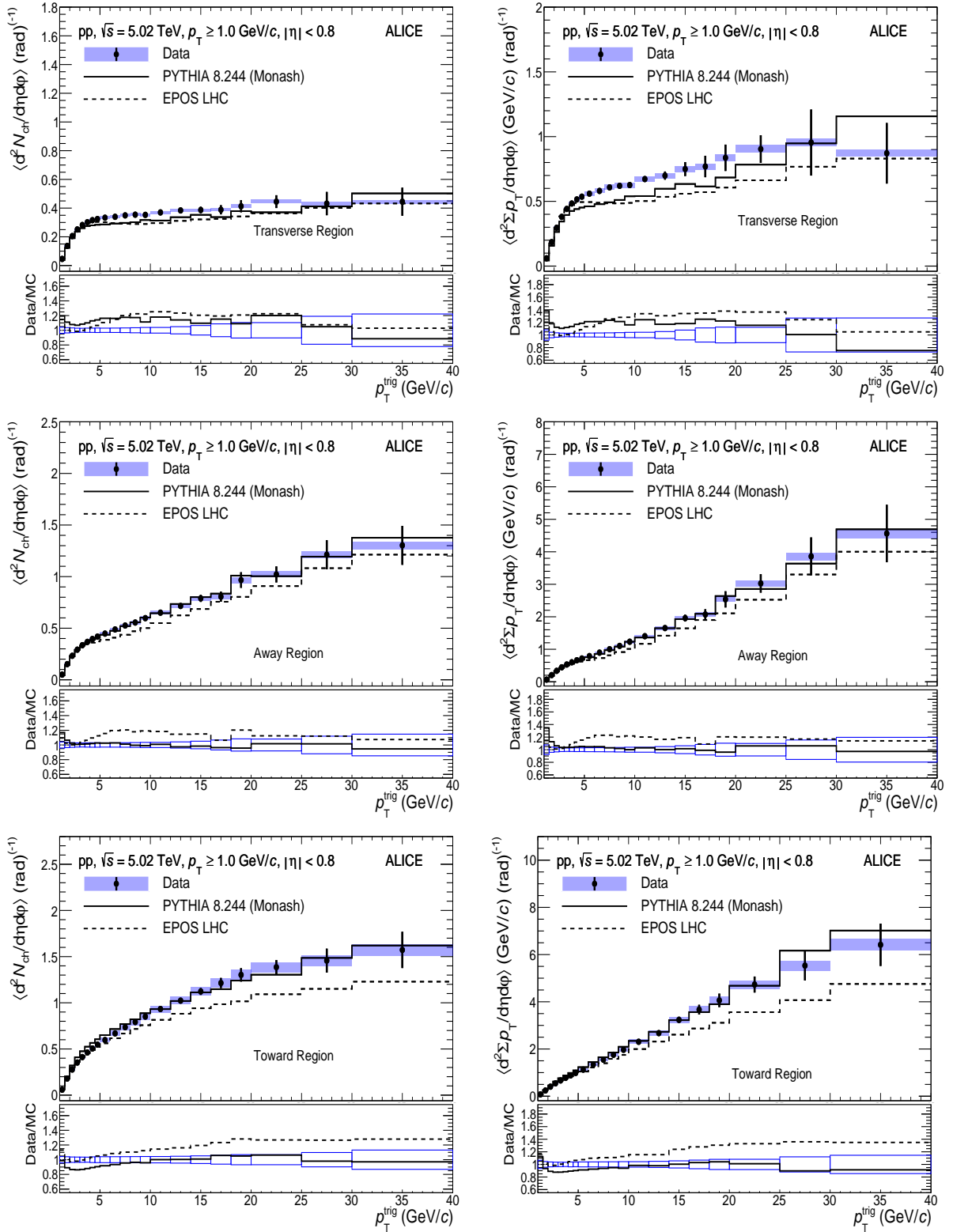


**Figure A.2:** The charged-particle number (left) and summed- $p_T$  (right) densities as a function of  $p_T^{trig}$  in pp collision at  $\sqrt{s} = 5.02$  TeV are displayed. Results for the transverse (top), away (middle), and toward (bottom) regions were obtained for the transverse momentum threshold  $p_T > 1$  GeV/c. The shaded area and the error bars around the data points represent the systematic and statistical uncertainties, respectively. Data are compared with PYTHIA 8/Monash (solid line) and EPOS LHC (dashed line) predictions. The data-to-model ratios are displayed in the bottom panel of each plot. The boxes around unity represent the statistical and systematic uncertainties added in quadrature.



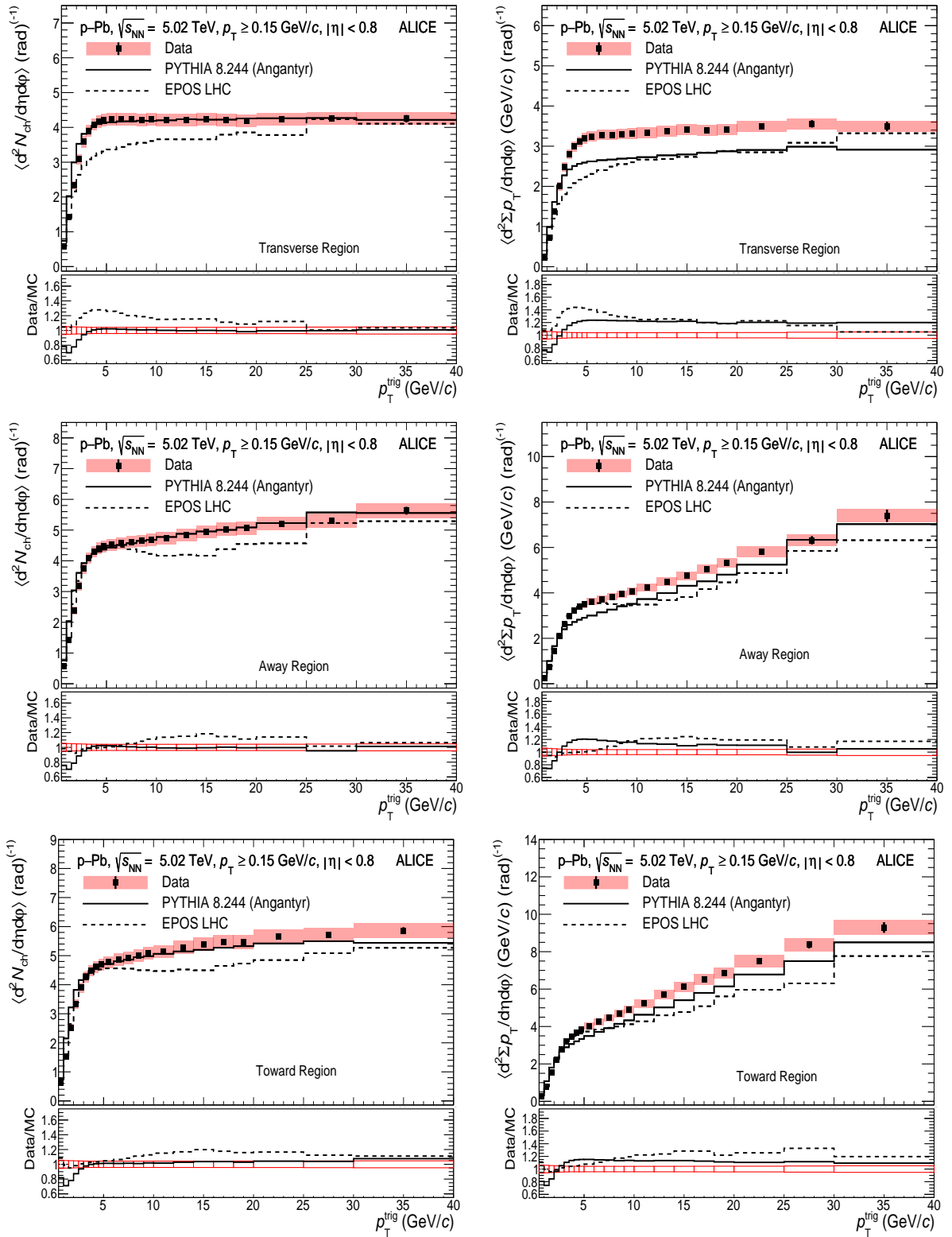


**Figure A.3:** The charged-particle number (left) and summed- $p_T$  (right) densities as a function of  $p_T^{\text{trig}}$  in p–Pb collision at  $\sqrt{s_{NN}} = 5.02$  TeV are displayed. Results for the transverse (top), away (middle), and toward (bottom) regions were obtained for the transverse momentum threshold  $p_T > 0.15$  GeV/c. The shaded area and the error bars around the data points represent the systematic and statistical uncertainties, respectively. Data are compared with PYTHIA 8/Angantyr (solid line) and EPOS LHC (dashed line) predictions. The data-to-model ratios are displayed in the bottom panel of each plot. The boxes around unity represent the statistical and systematic uncertainties added in quadrature.

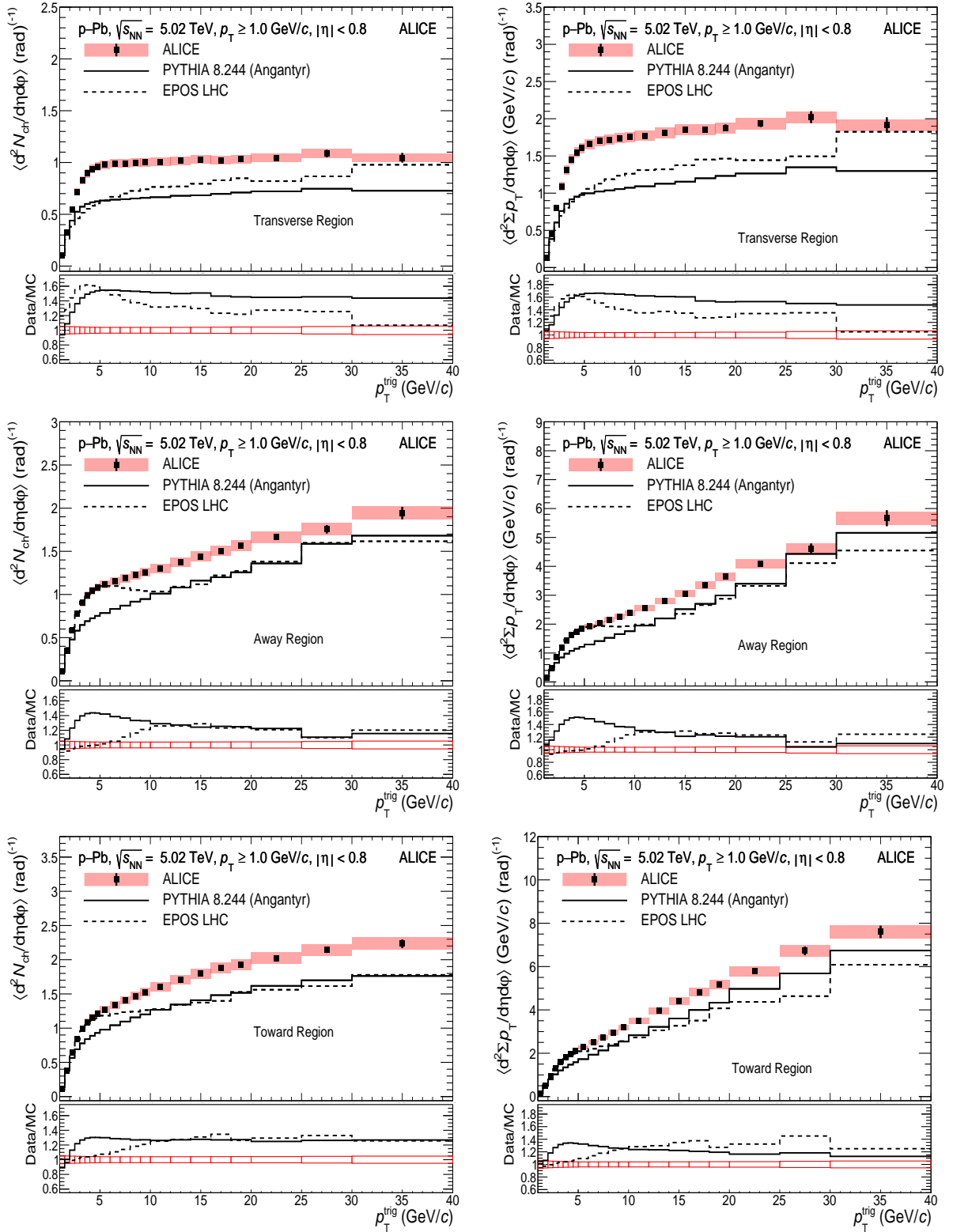


**Figure A.4:** The charged-particle number (left) and summed- $p_T$  (right) densities as a function of  $p_T^{trig}$  in p-Pb collision at  $\sqrt{s_{NN}} = 5.02$  TeV are displayed. Results for the transverse (top), away (middle), and toward (bottom) regions were obtained for the transverse momentum threshold  $p_T > 1$  GeV/c. The shaded area and the error bars around the data points represent the systematic and statistical uncertainties, respectively. Data are compared with PYTHIA 8/Angantyr (solid line) and EPOS LHC (dashed line) predictions. The data-to-model ratios are displayed in the bottom panel of each plot. The boxes around unity represent the statistical and systematic uncertainties added in quadrature.